IOP Publishing Biomed. Mater. 11 (2016) 015009 doi:10.1088/1748-6041/11/1/015009

Biomedical Materials

OPEN ACCESS

RECEIVED
30 October 2015

ACCEPTED FOR PUBLICATION
15 December 2015

PUBLISHED
2 February 2016

PAPER

On the interactions of human bone cells with Ti6Al4V thermally oxidized by means of laser shock processing

Lara Crespo[1,2], Margarita Hierro-Oliva[3,2], Sandra Barriuso[4], Virginia Vadillo-Rodríguez[3,2], M Ángeles Montealegre[5], Laura Saldaña[1,2], Enrique Gomez-Barrena[1,6], José Luis González-Carrasco[4,2], María Luisa González-Martín[3,2] and Nuria Vilaboa[1,2]

[1] Hospital Universitario La Paz-IdiPAZ, Paseo de la Castellana 261, 28046 Madrid, Spain
[2] CIBER de Bioingeniería, Biomateriales y Nanomedicina (CIBER-BBN), Spain
[3] Departamento de Física Aplicada, Universidad de Extremadura, Avda. de Elvas s/n, 06006 Badajoz, Spain
[4] Centro Nacional de Investigaciones Metalúrgicas, CENIM-CSIC, Avda. Gregorio del Amo 8, 28040 Madrid, Spain
[5] Centro Tecnológico AIMEN, Centro de Aplicaciones Láser, C/ Relva 27A-Torneiros, 36410 Porriño, Spain
[6] Departamento de Cirugía, Universidad Autónoma de Madrid, Calle del Arzobispo Morcillo 4, 28029 Madrid, Spain

E-mail: nuria.vilaboa@salud.madrid.org

Keywords: titanium alloy, laser, oxidation, mesenchymal stem cell, osteoblast

Abstract

We investigated a Ti6Al4V alloy modified by means of laser peening in the absence of sacrificial coatings. As a consequence of the temperature rise during laser focusing, melting and ablation generated an undulated surface that exhibits an important increase in the content of titanium oxides and OH− ions. Human mesenchymal stem cells and osteoblasts cultured on the oxidized alloy develop noticeable filopodia and lamellipodia. Their paxillin-stained focal adhesions are smaller than in cells attached to the untreated alloy and exhibit a marked loss of colocalization with the ends of actin stress fibers. An important imbalance of phosphorylation and/or dephosphorylation of the focal adhesion kinase is detected in cells grown on the oxidized alloy. Although these mechanisms of adhesion are deeply altered, the surface treatment does not affect cell attachment or proliferation rates on the alloy. Human mesenchymal stem cells cultured on the treated alloy in media containing osteogenic inducers differentiate towards the osteoblastic phenotype to a higher extent than those on the untreated surface. Also, the specific functions of human osteoblasts cultured on these media are enhanced on the treated alloy. In summary, laser peening tailors the Ti6Al4V surface to yield an oxidized layer with increased roughness that allows the colonization and activities of bone-lineage cells.

1. Introduction

Ti6Al4V alloy (Ti64) is the metallic biomaterial most commonly used for manufacturing bone-anchoring devices due to its favourable combination of biocompatibility, mechanical strength and corrosion resistance. The spontaneous formation of a surface passive film, typically amorphous and non-stoichiometric TiO_2, provides good corrosion resistance and low rates of metal ion release. The poor adhesion of the protective passive film to the substrate, however, results in alteration of the stability of the passive layer under friction conditions. Repassivation of the alloy is very fast, but with increasing time the continuous passivation–repassivation processes consume metal and increase the roughness, which accounts for the poor abrasive and adhesive wear resistance of the alloy even during friction with tissues. Engineering technologies to produce oxide layers resilient to both chemical and mechanical attack include thermal oxidation, a cost effective and environmentally friendly surface treatment that generates highly crystalline rutile (TiO_2) layers on even or rough Ti64 surfaces [1, 2]. Short-term oxidation treatments of the polished alloy at 500–700 °C in air yield thick TiO_2 layers, up to 1 μm, that effectively decrease ion release [3], improve the corrosion behaviour [1, 4–7] and enhance the interactions of bone-forming cells with the alloy [4, 8]. A limitation of thermal oxidation processing is that the full component is necessarily subject to treatment, which may cause thermal stability loss of the alloy microstructure, carefully designed to achieve

optimal mechanical properties, and relief of the subsurface compressive residual stress state. The net effect may be a drastic decrease of the fatigue strength. Therefore, a window of opportunity is envisaged for treatments of Ti64 that promote surface oxide formation without compromising its bulk properties.

Laser shock processing, also known as laser peening (LP), is an innovative surface processing technology in which metallic surfaces are irradiated with short and intensive laser pulses. Irradiation by high power laser pulses induces high pressure plasma, of the order of gigapascals, which produces high amplitude shock waves. The net effect on the material is the development of compressive residual stresses that extend deeper below the surface than, for instance, conventional shot peening [9] or grit blasting [10] treatments, with a reduced work hardening close to the surface. Subsurface induced effects may improve the fatigue strength by up to about 10–40% [11]. To increase the efficiency of LP, the treated samples are usually coated with a laser-energy absorbing coat, known as a sacrificial or ablative layer, which is covered with a transparent layer or immersed in water. With the use of water confinement, the thermal expansion of the plasma is trapped and the pressure against the surface of the workpiece increases by a factor of five to ten [12]. Depending on the LP parameters and the characteristics of the metallic material, the surface may experience topographical changes.

Fatigue is a type of damage frequently experienced by metals and an important cause of failure of orthopaedic and dental Ti64-based implants [13–16]. In fact, LP has been previously applied to Ti64 surfaces and the beneficial effects on their mechanical properties have been described [17–19]. For biomedical applications, LP cannot employ sacrificial layers as they may cause surface contamination. In the absence of ablative coating, thermal rise at the Ti64 surface during laser focusing is extremely high, which may lead to oxidation of the outer alloy surface. However, the chemical changes experienced by the Ti64 surface after LP without protective coating have not been reported to date. The response of bone cells to laser shock processed Ti64 surfaces, essential to predict whether the treated alloy might be used for the fabrication of implantable medical devices, has not been investigated either.

This study describes the surface properties of an LP-treated Ti64 alloy and reports on the interactions of human osteoblasts and their precursors, mesenchymal stem cells from bone marrow, with the treated alloy. For comparison purposes, Ti64 samples in the as-polished state were also investigated.

2. Materials and methods

2.1. Sample preparation

Disks of 2 mm thickness were cut by electrospark erosion from a hot-rolled and annealed (700 °C) bar of Ti64 ELI (extra low interstitial) alloy 21 mm in diameter, supplied by Surgival SL (Valencia, Spain). The chemical composition of the alloy in weight percent is 6.1 Al, 4.2 V, 0.12 O, 0.01 C, 0.006 N, balance Ti, as indicated in the analysis certificate. The surface of the disks was ground with silicon carbide papers of decreasing grain size and then finely polished with diamond paste of 1 μm particle size to get a mirror-like finish. Finally, samples were rinsed in a jet of warm water prior to sonication in alcohol. Polished samples, used as a control, will be referred to as Ti64. Another set of disks was ground with 2400 grit silicon carbide paper and then irradiated with a PRO 290-30 *Q*-switched Nd-YAG laser from Quanta Ray Spectra Physics working in the fundamental harmonic at 1.6 J/pulse and producing pulses of 10 ns. The processed samples were placed in a holder with a programmable *XYZ* positioning system to generate the path of laser pulses, as shown in figure 1(a). Samples were irradiated at a density of 421 pulses cm^{-2}. The laser beam was guided by a mirror, focusing it with a lens and generating spots of 2.4 mm in diameter with an overlap of 80%. Water was used as the confining medium. Laser-treated specimens were cleaned following the procedure described above. These samples will be referred to as Ti64 LP.

Ti64 and Ti64 LP specimens were washed in distilled water and then sterilized under ultraviolet light before cell culture experiments.

2.2. Material characterization

Microstructural analyses of Ti64 and Ti64 LP samples were performed by scanning electron microscopy (SEM), using a JEOL JSM6500F field emission gun electron microscope (Peabody, MA, USA) equipped with an energy dispersive x-ray system (EDR288, Rontec, Berlin, Germany). Both secondary and backscattered electrons were collected for imaging the surface of the samples.

A D8 Discover diffractometer (Bruker AXS, Karlsruhe, Germany) equipped with Goebel mirror optics and a Co tube was used for x-ray diffraction (XRD) measurements. A voltage of 40 kV and a current of 30 mA were used in grazing incidence condition and a conventional $\theta - 2\theta$ scan to determine both crystal microstructure and depth profiling. In both cases, the AbsorbDX software (Bruker AXS) was used to calculate the thickness at which 90% of the x-rays are scattered, $t_{0.9}$. For an incidence angle of 1° and Co K_α radiation, $t_{0.9}$ was about 0.3 μm, while in the case of the $\theta - 2\theta$ scan $t_{0.9}$ values were about 3.28 and 5.96 μm for the (1 0 1) and (2 0 1) diffraction peaks, respectively. Selected operational conditions provided x-ray diffraction diagrams with narrow peaks and sufficient counting statistics. In both types of scan, XRD data were collected in the 30–110° 2θ range, with a step size of 0.03°. The JCPDS database and the DIFFRACplus EVA software (Bruker AXS) were used to identify the phases in XRD patterns. Instrument functions were empirically parameterized for both $\theta - 2\theta$ scans and grazing incidence from the XRD patterns of a corundum plate

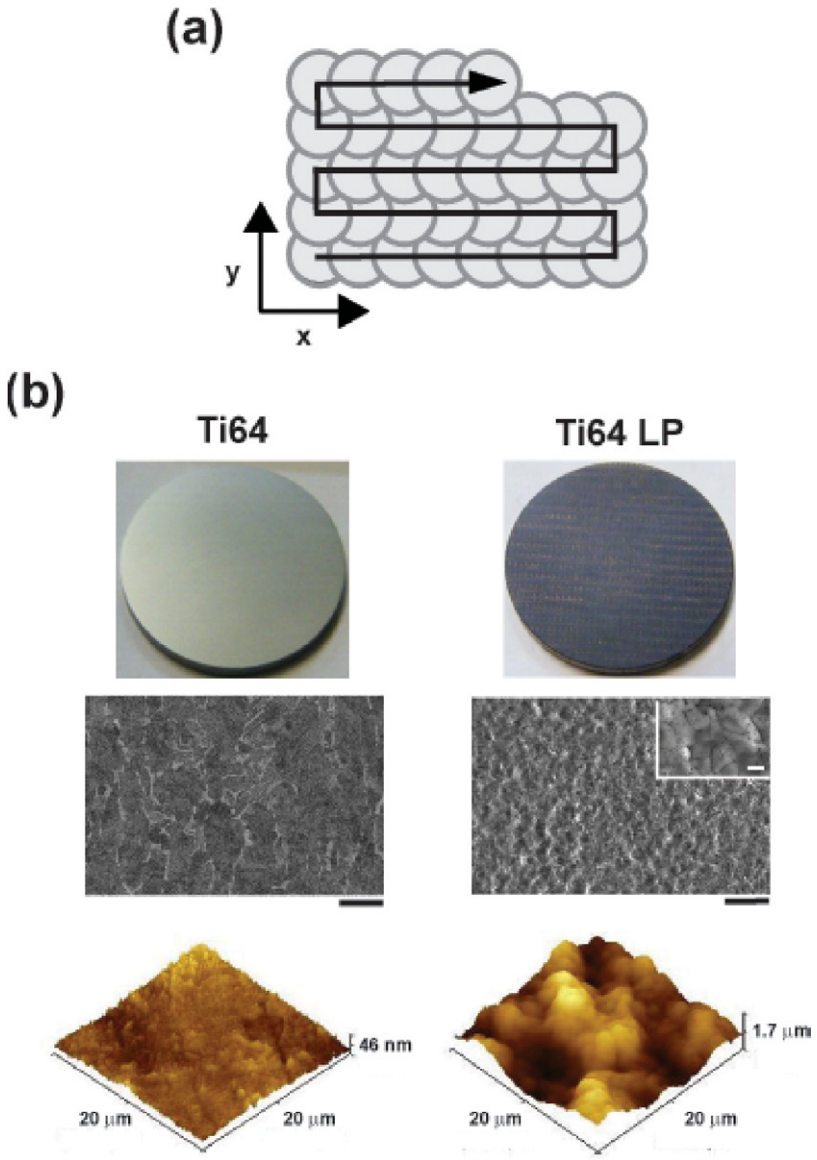

Figure 1. Topographical features of Ti64 LP surfaces. (a) Scheme of the laser beam path used to process the Ti64 samples, which generates overlapped spots. (b) Topographical features of Ti64 LP surfaces. Gross appearance of Ti64 and Ti64 LP (upper panel), SEM images of Ti64 obtained by backscattered electrons and of Ti64 LP obtained by secondary electrons (middle panel) and AFM images in topographic mode (bottom panel). Bar, 200 μm. Bar in magnified SEM images, 20 μm.

sample. XRD data refinement was performed using version 4.2 of the Rietveld analysis program TOPAS (Bruker AXS). Background, zero displacement, peak breadth, scale factors, texture parameters and the unit cell parameter were considered in the refinement protocol, using room temperature (RT) structures that were a combination of the phases present in the base materials.

Surface topography analysis was initially carried out by means of mechanical profilometry using a Mitutoyo Surftest 201 analyzer (Mituyoto America, Aurora, IL, USA). The measurements were obtained from three independent line profiles of 4 mm measurement length, using a diamond stylus tip of 5 μm diameter under 4 mN load at a tracing speed of 0.5 mm s^{-1}. Profilometer scans were performed perpendicular to the path of laser pulses. R_a, which is the average surface roughness parameter that corresponds to the arithmetic mean of all deviations from the line over the sampling path, and R_z, which is the average distance between the five highest peaks and the five deepest valleys within the sampling length, were calculated. High-resolution roughness measurements were made using atomic force microscopy (AFM). AFM topographical images were obtained with an Agilent AFM 5500 system (Agilent Technologies, USA) operating at RT in contact mode using rectangular silicon cantilevers characterized by a spring constant and tip radius of 0.03 N m^{-1} and about 8 nm, respectively, according to the manufacturer's specifications (CSC38 series, Mikromash, Watsonville, CA, USA). The images were recorded in air at a constant scan rate of 2 Hz and applied force of 1 nN or less. For each sample, five topographical images were collected at randomly selected locations. R_{rms}, which is the average surface roughness parameter that corresponds to the geometric mean of all deviations from the line over the sampling path, and R_a associated to each topographical

image (scanned area of 20 × 20 μm^2) were calculated using offline software (Gwyddion version 2.26, David Nečas and Petr Klapetek, Czech Republic).

X-ray photoelectron spectroscopy (XPS) measurements were made using a K-Alpha Thermo Scientific instrument (Waltham, MA, USA) equipped with a monochromatic Al K_α x-ray source (1486.7 eV). The samples were investigated under ultrahigh vacuum conditions (3.5×10^{-8} mbar). The x-ray spot size was about 400 μm. The titanium surface was cleaned by 3 keV Ar^+ ion bombardment for 5 s to reduce the amount of carbon contamination. Survey spectra of the samples were collected and used to calculate atomic percentages of the elements present on the surface, and high resolution spectra of O 1s, C 1s, Al 2p and Ti 2p peaks were used to identify the chemical states of titanium and aluminium oxides. The pass energy for the survey spectra was 200 eV, whereas detailed spectra were taken with high resolution at 50 eV pass energy. The binding energy (BE) values were referenced by setting the C 1s BE to 285 eV and the XPS spectra were background subtracted using the Shirley method and deconvoluted using a mixed Gaussian/Lorentzian peak shape with XPSPeak software (version 4.1). This software provides the position, area, full width at half maximum and Gaussian/Lorentzian ratio, taking into account the asymmetry of each of the analyzed peaks.

Time of flight secondary ion mass spectrometry (Tof-SIMS) analyses of the surfaces were performed using a Tof-SIMS5 (ION TOF, Münster, Germany) equipped with a Bi^+ primary gun operated at 25 kV. The total ion dose used to acquire each spectrum was above 10^{12} ions cm^{-2}. Negative spectra were recorded from 0 to 850 a.m.u. The depth profile was recorded using a 2 kV Cs^+ sputter beam, which was rastered over a 250 μm × 250 μm area for acquisition times of 500 and 1500 s for Ti64 and Ti64 LP samples, respectively. A pulsed low energy electron flood gun was used for charge neutralization. The secondary ion species analyzed were OH−, AlO−, TiO− and TiO_2−. The depth reached in samples after sputtering was estimated by measuring the depth of several SIMS craters via optical profilometry, using an Optical Profiler Zeta-20 (Zeta Instruments, San Jose, CA, USA).

2.3. Cell culture

Purified human mesenchymal stem cells (hMSCs) were purchased from Lonza (Basel, Switzerland). Experiments were performed using six different batches of hMSCs obtained from donors aged 18–28 years. hMSCs were expanded in a defined medium (Lonza), which includes MSC basal medium and the SingleQuots© growth supplements containing heat inactivated fetal bovine serum (FBS), penicillin/streptomycin and L-glutamine. hMSCs were routinely analyzed by flow cytometry analysis for various cell surface markers, CD105 +, CD29 +, CD44 +, CD14 +, CD34 + and CD45 +, commonly used for the characterization of mesenchymal stem cells (data not shown), as previously described [20]. Experiments were carried out with hMSCs cultured up to the seventh passage.

Primary cultures of human osteoblasts (hOBs) were isolated as described previously [8] from trabecular bone explants collected from six different patients, aged 69–80 years, undergoing orthopaedic knee surgery. All procedures were approved by the Human Research Committee of Hospital Universitario La Paz (date of approval: 16 April 2009). An informed consent form was signed by the participants enrolled in this study. Bone fragments from independent patients were processed in separate primary cultures and maintained in Dulbecco's modified Eagle's medium (DMEM) (Lonza) supplemented with 15% (v/v) FBS, 0.1 mg ml^{-1} streptomycin and 500 UI ml^{-1} penicillin. Once cultures reached confluence, hOBs were subcultured from initial isolates for subsequent experiments, which were carried out using independent cultures from different patients.

hOBs and hMSCs were maintained in a humidified incubator at 37 °C, under 5% CO_2.

2.4. Cell attachment assays

For cell attachment assays, hMSCs and hOBs were seeded on the samples at a density of 1.4×10^4 cells cm^{-2} in DMEM medium containing 15% FBS and antibiotics. After culturing for 2, 4, 15 or 24 h, cells were gently washed with phosphate-buffered saline (PBS) and fixed with a solution of 2.5% glutaraldehyde in PBS. Attached cells were observed using a confocal microscope (Leica TCS SPE, Leica Microsystems, Wetzlar, Germany). The autofluorescent signal due to glutaraldehyde fixation was excited with a 488 nm laser line and collected in the emission range 495–590 nm. The number of cells attached to the samples was quantified in ten representative images, which covered a surface area of 727 × 727 μm^2, using ImageJ version 1.34 image analysis software (http://rsbweb.nih.gov/ij).

2.5. Scanning electron microscopy

Cells were seeded on the samples at a density of 1.4×10^4 cells cm^{-2} and cultured for 4 h in DMEM medium containing 15% FBS and antibiotics. After washing with PBS, attached cells were fixed in 2.5% glutaraldehyde for 1 h at RT. After dehydrating through a graded ethanol series (30–100%, v/v), the samples were critical point dried with CO_2 (Quorum Technologies CPD7501, UK), gold sputter-coated on a rotating–tilting stage (Sputter Coater SC510, Bio-Rad, Spain), and then examined by SEM (FEI Quanta 200 ESEM, Hillsboro, OR, USA).

2.6. Cell viability assays

Cells were seeded at a density of 1.4×10^4 cells cm^{-2} on the samples and cultured for up to 7 d, in DMEM medium containing 15% FBS and antibiotics. Cell viability was evaluated at 1, 4 and 7 d of culture using the alamarBlue assay (Biosource, Nivelles, Belgium).

Cells were washed with PBS and then incubated in culture medium containing 10% (v/v) alamarBlue dye for 3 h at 37 °C. Media were collected and, after excitation at 530 nm, emitted fluorescence at 590 nm was quantified using a Synergy4 microplate reader (BioTek Instruments, Winooski, VT, USA).

2.7. Immunofluorescence assays and analysis of focal adhesions

Cells were seeded on the samples at a density of 1.4×10^4 cells cm^{-2} and cultured in DMEM medium containing 15% FBS and antibiotics. After the indicated periods of time, cells were washed with PBS followed by fixation in 4% (w/v) paraformaldehyde in PBS and permeabilization with 0.1% Triton X-100 in PBS. Cells were blocked in 2% bovine serum albumin (BSA, Sigma-Aldrich, Madrid, Spain) in PBS containing 0.05% Tween 20 and then incubated with mouse anti-human fibronectin (FN) monoclonal antibody (mAb) (Chemicon, Harrow, UK) diluted 1:100, mouse anti-human paxillin mAb (Becton Dickinson Biosciences, Madrid, Spain) diluted 1:200, mouse anti-human focal adhesion kinase phosphorylated at Tyr-397 (p-FAK Y397) polyclonal antibody (pAb) (Chemicon) diluted 1:50 (v/v) and rabbit anti-human focal adhesion kinase phosphorylated at Tyr-407 (p-FAK Y407) pAb (Biosource) diluted 1:50 (v/v) in 1% BSA in PBS. Cells were washed with 0.05% Tween 20 in PBS followed by incubation with goat anti-mouse or anti-rabbit Alexa-Fluor 488 (Molecular Probes, Leiden, Holland) diluted 1:1000 (v/v) in 1% BSA in PBS. To label actin cytoskeleton, cells were additionally incubated with PBS containing 4×10^{-7} M phalloidine-TRITC (Sigma-Aldrich). After washing with PBS containing 0.05% Tween 20, cells were imaged using a confocal microscope (Leica TCS SPE). To quantify the length of paxillin in focal adhesions, a total of 250 adhesions randomly selected from four representative images per sample, from two experiments with similar results, were analyzed using ImageJ version 1.34 image analysis software.

2.8. p-FAK Y397 level measurements

Cells were seeded on the samples at a density of 1.4×10^4 cells cm^{-2} and cultured for 15 h in DMEM containing 15% FBS and antibiotics. Cell layers were washed exhaustively with PBS, extracted with 10^{-1} M Tris-HCl pH 7.4, 10^{-1} M NaCl, 10^{-3} M EDTA, 10^{-3} M EGTA, 10^{-3} M NaF, 2×10^{-2} M $Na_4P_2O_7$, 2×10^{-3} M Na_3VO_4, 1% Triton X-100, 10% glycerol, 0.1% SDS, 0.5% deoxycholate, 10^{-3} M PMSF and a protease inhibitor cocktail (Complete, Roche Applied Sciences, Indianapolis, IN, USA). Cell lysates were clarified by centrifugation and stored at −80 °C. p-FAK Y397 levels were quantified in clarified extracts using a specific immunoassay kit (Invitrogen, Carlsbad, CA, USA), with a sensitivity of 0.045 U. One unit is equivalent to the amount of p-FAK Y397 autophosphorylated from 300 pg of total FAK protein. p-FAK Y397 levels were normalized to the total protein amounts in cell lysates, determined using the Bio-Rad protein assay (Bio-Rad Laboratories, Hercules, CA, USA) and using BSA as standard.

2.9. Differentiation and maturation assays

Cells were seeded on the samples at a density of 1.4×10^4 cells cm^{-2} in DMEM containing 15% FBS and antibiotics. After 24 h, medium was replaced with osteogenic medium, consisting of DMEM supplemented with 15% FBS, 10^{-7} M dexamethasone, 3×10^{-4} M ascorbic acid, 10^{-2} M β-glycerophosphate (Sigma-Aldrich) and antibiotics, and cells were further cultured for 13 d. This incubation period is enough to detect a mineralized matrix layer, as Raman spectroscopy analyses can identify signal of hydroxyapatite at 960 cm^{-1} as early as 9 d after incubating hMSC in osteogenic medium [21]. Media were partially replaced every 3 d to avoid exhaustion of nutrients. To quantify the degree of cell layer calcification, cells were extensively washed with PBS, fixed with ethanol and then stained with a solution of 4×10^{-2} M Alizarin Red S in deionized water (pH 4.2). Excessive dye was removed by rinsing with deionized water. The retained stain was eluted with 10% (w/v) cetylpyridinium chloride and the absorbance at 562 nm was quantified using a microplate reader (Synergy 4). Parallel cultures were washed with PBS and cells were extracted in 5×10^{-1} M NaCl, 5×10^{-2} M Tris-HCl pH 8.0 and 1% Triton X-100 supplemented with a mixture of protease inhibitors containing 50 $\mu g\,ml^{-1}$ bacitracin, 17.5 $\mu g\,ml^{-1}$ phenyl-methylsulfonylfluoride, 1 $\mu g\,ml^{-1}$ pepstatin A and 2 $\mu g\,ml^{-1}$ aprotinin (all from Sigma-Aldrich). Alkaline phosphatase (ALP) activity was quantified in cell extracts by measuring the release of p-nitrophenol from p-nitrophenylphosphate (Sigma-Aldrich) at 37 °C and pH 10.5. Protein concentrations of lysates were determined using the Bio-Rad protein assay to permit normalization of ALP activity data. To visualize osteocalcin in the cell matrix, cells were cultured for 21 d in osteogenic medium and immunostained with mouse anti-human osteocalcin pAb (Biogenesis, Poole, England) diluted 1:100 (v/v) in 1% BSA in PBS, as indicated in section 2.7.

2.10. Statistical analysis

Data are expressed as mean ± standard deviation (SD) of six independent experiments. The differences between Ti64 and Ti64 LP samples were evaluated using the non-parametric Mann–Whitney U test. Statistical analyses were carried out at the $p < 0.05$ level of significance, using the Statistical Package for the Social Sciences version 15 (SPSS, Chicago, IL, USA).

3. Results

3.1. Material characterization

Optical examination of Ti64 samples processed by means of LP reveals that they undergo discolouration to

Table 1. Chemical composition (mass %) of the investigated surfaces as determined by XRD analyses ($\theta - 2\theta$ scan).

	α-phase	β-phase	TiO
Ti64	86	14	—
Ti64 LP	65	22	13

bluish, indicating possible formation of an oxide layer on the surface (figure 1(b), upper panel). Also, traces of the generated spots and the path of the laser beam can be clearly distinguished on treated surfaces. SEM analysis of Ti64 samples reveals the duplex microstructure of the alloy characterized by a dark phase of primary α grains, about 4 μm width, and Widmanstätten $\alpha + \beta$ colonies. Bright contrast corresponds to β phase, which contains a higher amount of vanadium and thus a higher average atomic number. However, a closer examination of Ti64 LP samples indicates the formation of an even scale, tightly adhered to the substrate, without signs of spallation (figure 1(b), middle panel). As shown in magnified secondary electron images, the topography of Ti64 LP surface is characterized by a wavy surface of small grains of about 2–3 μm in size, often containing submicrometer voids, and occasionally separated by small cracks. Mechanical profilometry confirmed the changes in roughness of the LP-treated surface. Thus, R_a and R_z values in Ti64 were 6 $\pm$ 1 and 31 $\pm$ 3 nm, respectively, and increased to 0.17 $\pm$ 0.01 and 1.16 $\pm$ 0.07 μm in Ti64 LP. The topography was also analyzed at a closer scale by AFM, which revealed a mixture of convex and concave surface features (figure 1(b), bottom panel). Measured within a scanned area of 20 $\times$ 20 μm^2, the surface of Ti64 LP exhibits large features protruding from the surface together with cavities that increase R_a and R_{rms} to 0.227 $\pm$ 0.028 and 0.290 $\pm$ 0.03 μm, respectively. However, the Ti64 surface exhibits very low R_a and R_{rms} values, down to 2.7 $\pm$ 0.4 and 3.8 $\pm$ 0.7 nm, and displays a high density of spikes of nanometric dimensions.

The nature of the scale was determined by XRD ($\theta - 2\theta$ scan). Analysis of the Ti64 LP sample revealed the presence of the α and β phases, corresponding to the substrate, and a small percentage of metastable TiO (ccc) with a lattice parameter of 4.16 Å (table 1).

The chemical compositions of the outermost layers of Ti64 and Ti64 LP surfaces were analyzed by XPS. Figure 2(a) shows the high resolution spectra of Ti 2p and Al 2p. In both samples, a main Ti^{4+} $2p_{3/2}$ peak at 458.2 eV is detected, with 5.7 eV splitting between the Ti $2p_{1/2}$ and Ti $2p_{3/2}$ peaks, which are related to TiO_2. An additional intensity contribution to the Ti 2p region is observed in Ti64 LP, in the area where the Ti^{3+} (Ti_2O_3) doublet is expected, with BE = 456.4 eV for the Ti $2p_{3/2}$ peak and with 5.5 eV splitting between the Ti $2p_{1/2}$ and Ti $2p_{3/2}$ peaks. This contribution can be also observed in Ti64, but with a much lower intensity than for Ti64 LP, together with a small contribution from Ti^0 from the bulk metallic titanium. These results indicate that the oxide layer developed on the Ti64 LP sample is thicker than the passive film grown on Ti64 and contains an important amount of Ti_2O_3. The shape and position of the Al 2p peak show that Al is present mainly as Al^{3+} (Al_2O_3) on Ti64 and Ti64 LP samples. However, another contribution to the Al 2p region, which can be assigned to Al–OH, was detected in Ti64 LP surfaces.

TOF-SIMS depth profiles of AlO−, OH−, TiO− and TiO_2− revealed that these secondary ions are located considerably deeper in Ti64 LP than in Ti64 surfaces. The longer sputtering time needed to achieve nearly oxide ion null contributions in Ti64 LP surfaces is also noticeable. Profilometry measurements of several SIMS craters generated after different sputtering times allow a rough estimation of the depth of the oxide layer. Assuming a linear dependence between depths of craters and sputtering time, the erosion rate of Ti64 is six times higher than the rate of Ti64 LP. Thus, oxides decrease to their half values within a depth range which is about ten times higher for Ti64 LP than for Ti64. Remarkably, OH− ions increase to a large extent and become deeper in Ti64 LP as a consequence of the water confinement of samples during treatment. In agreement with the expected distribution of titanium oxides, TiO_2− has its maximum at very short sputter time, but the TiO− ion, which may arise from any titanium oxide, reaches a maximum after more than 100 s sputtering. These results indicate that titanium oxides, detected in the outermost layer of Ti64 LP by means of XPS, are less saturated in oxygen as the depth of the oxidized layer increases, due to lower oxygen availability. Similarly, the maximum for the AlO− ion is found at the same sputter time as for the TiO− ion. However, AlO− has a very narrow relative maximum at the shortest sputter time that could be related to the presence of aluminium hydroxide, as shown in the XPS spectrum.

3.2. Cell adhesion to laser-peened Ti64 surfaces

Cell attachment assays were conducted after incubating cells for 2, 4 and 15 h on Ti64 and Ti64 LP samples (figure 3(a)). The number of adhered cells increased with time on both surfaces regardless of the cell type, although some differences were detected in the adhesion rates of bone-forming cells and stem cells. hMSCs adhered more rapidly than hOBs. There was an increase in hMSC attachment between 2 and 4 h of incubation, but not in hOBs. However, a substantial increase in hOB attachment occurred after 4 h, the number of hMSCs remaining constant. Interestingly, the numbers of hMSCs or hOBs attached to Ti64 and Ti64 LP surfaces at the three examined time points were similar. As observed by SEM, hMSCs and hOBs cultured on Ti64 for 4 h were well spread and flat, exhibiting a round shape due to the formation of extensive lamellipodia that protruded in all directions (figure 3(b)). Cells appeared stretched when cultured on Ti64 LP, with long filopodia anchored to the surface. The actin cytoskeleton, involved in the acquisition of cell shape and the formation of cellular protrusions,

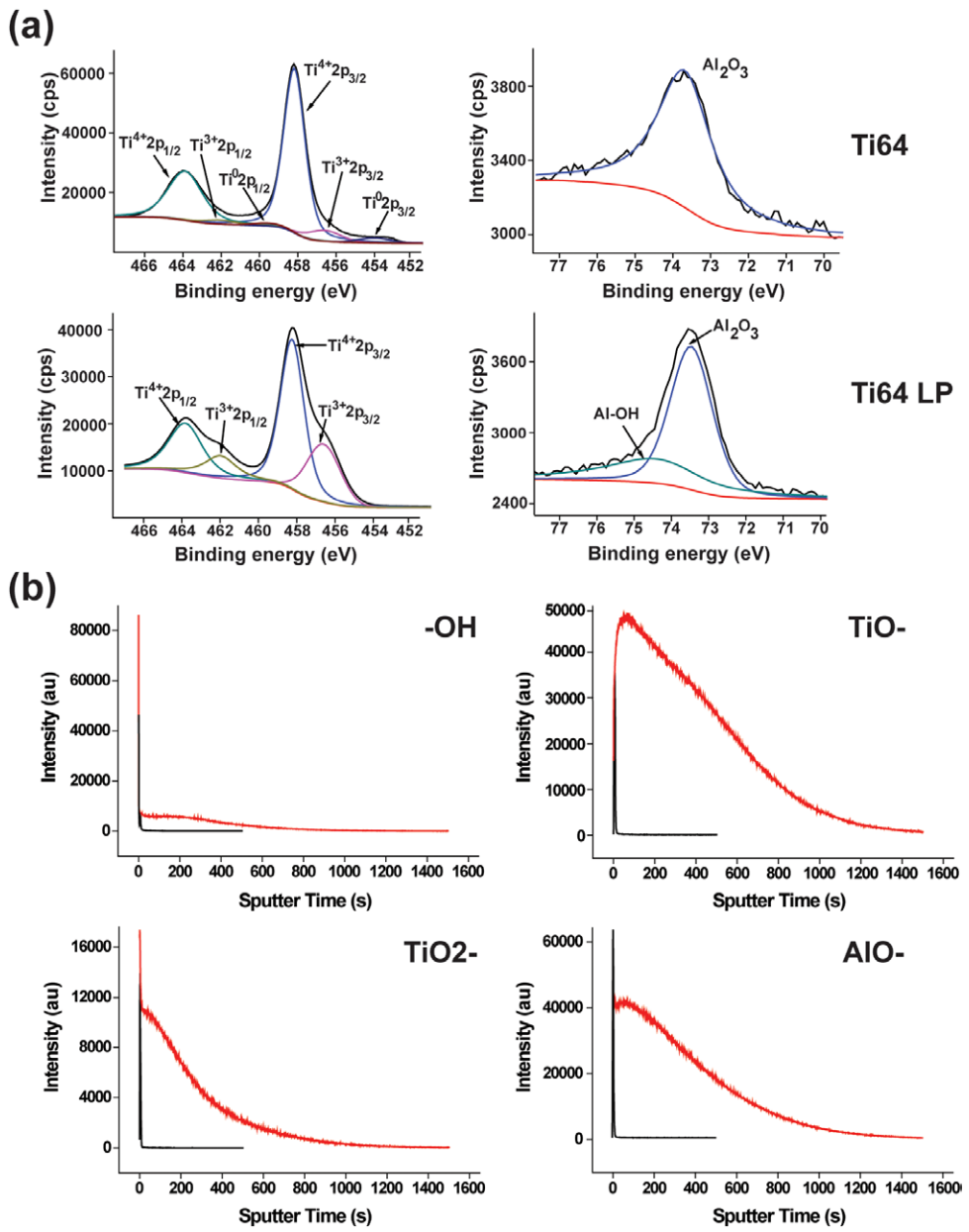

Figure 2. Chemical features of Ti64 LP surfaces. (a) High resolution XPS spectra of Ti 2p (left panels) and Al 2p (right panels) regions of Ti64 and Ti64 LP surfaces. (b) TOF-SIMS depth profiles of OH−, TiO−, TiO_2− and AlOTiO− secondary ions in Ti64 (black line) and Ti64 LP (red line) surfaces; au, arbitrary units.

showed important differences on the two studied surfaces (figure 3(c)). After 4 h of incubation on Ti64, both cell types arranged their actin filaments in a concentric pattern and displayed lamellipodia, sheet-like branched networks of criss-crossed actin filaments, as well as small microspikes and filopodia composed of unidirectional and parallel actin bundles pointing in random directions. On Ti64 LP, well defined actin bundles distributed through the cell body and aligned toward the cellular extensions. Also, long and fine cellular protrusions consisting of actin filament projections were visible at the attachment sites. When the incubation time on Ti64 increased, hMSCs and hOBs organized their actin cytoskeletons in thick bundles of stress fibers as cell shape evolved to the typical polygonal and elongated morphology. Cells cultured on Ti64 LP for 24 h maintained their stretched shapes and continued exhibiting long cell protrusions that ended in large lamellipodia with veil-like appearances. These structures were not observed in cells grown on Ti64.

3.3. Organization of focal adhesions on laser-peened Ti64 surfaces

To analyze the changes in the distribution of focal adhesions with time, hMSCs and hOBs were cultured for 4, 15 and 24 h on the surfaces and then double-stained for actin and paxillin, an adapter protein that localizes in adhesive structures upon attachment to the substrate (figure 4). Confocal images of both cell types cultured on Ti64 showed a marked peripheral distribution of focal adhesions, where paxillin

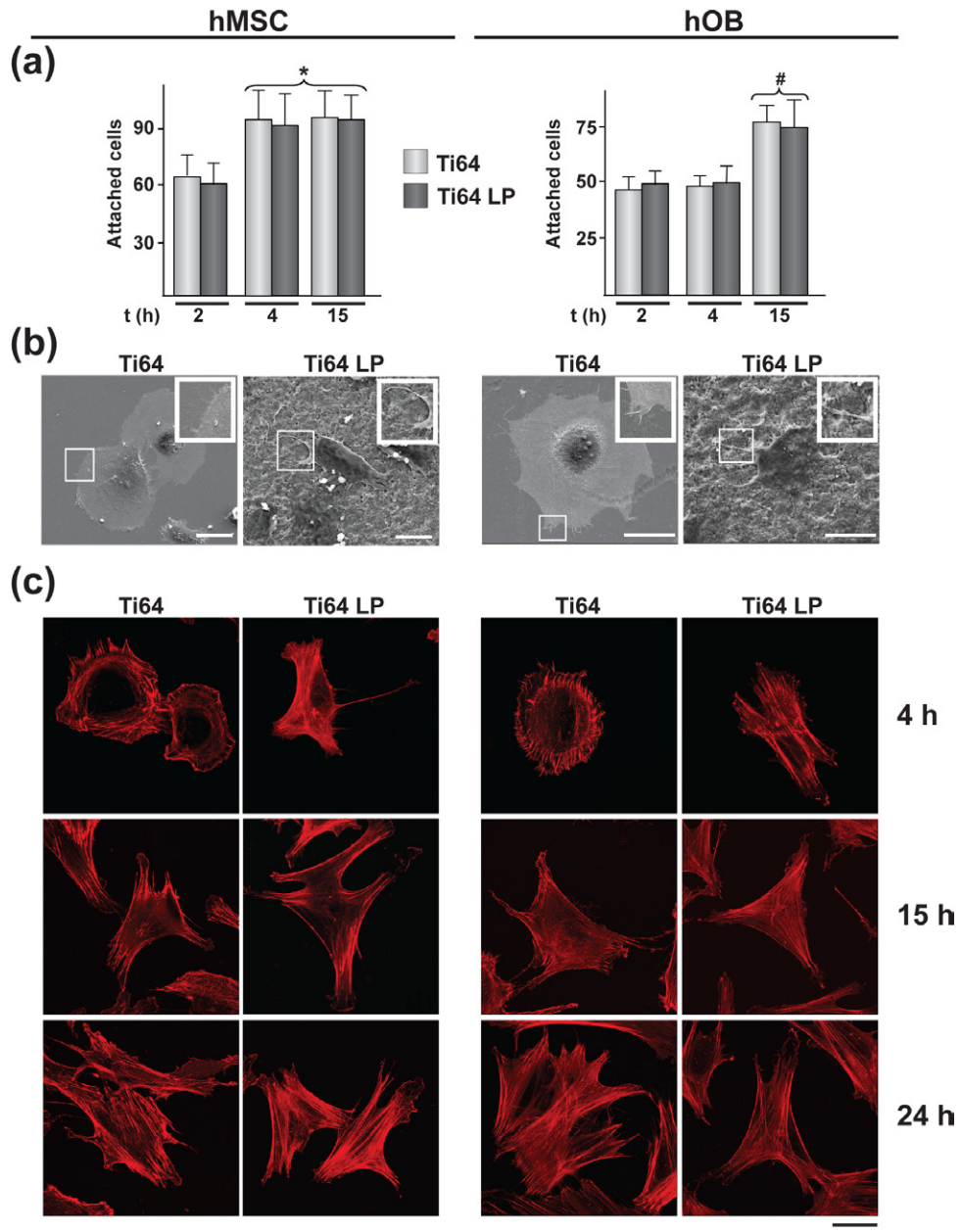

Figure 3. Cell adhesion to Ti64 LP surfaces. (a) hMSCs and hOBs were cultured for 2, 4 and 15 h on Ti64 and Ti64 LP surfaces and the number of attached cells was quantified in a surface area of 727 × 727 μm^2. Each value represents the mean ± SD of six independent experiments. $^{*}p < 0.05$ compared to cells cultured for 2 h on the same surface. $^{\#}p < 0.05$ compared to cells cultured for 2 and 4 h on the same surface. (b) SEM images of hMSCs and hOBs cultured for 4 h on Ti64 and Ti64 LP surfaces; bar, 25 μm. (c) Confocal maximum projections showing actin staining of hMSCs and hOBs cultured for 4, 15 and 24 h on Ti64 and Ti64 LP surfaces; bar, 40 μm. All images are representative of three independent experiments with similar results.

and the ends of actin filaments clearly colocalized. Colocalization of the two proteins was detected at the edges of lamellipodia of hMSCs and hOBs at the early time point of 4 h. At longer incubation times on Ti64, paxillin accumulated at the focal adhesions located at both ends of ventral stress fibers. On Ti64 LP surfaces, paxillin was recruited to the protrusive cell membrane structures but also showed diffuse cytoplasmic localization in both cell types. Fewer paxillin-stained areas, which appeared as dot-like structures, were detected in the periphery of cells (figure 5). Moreover, only some minor colocalization of paxillin with actin fibers was observed in the attachment sites, even in cells cultured for 24 h. Morphometric analysis of paxillin-stained areas confirmed that focal adhesion length decreases in hMSCs and hOBs cultured on Ti64 LP (figure 5). Next, we investigated the distribution of the active form of FAK, a central regulator of the assembly of focal adhesions, in cells cultured for 15 h on the alloy surfaces. As with paxillin, there was a marked accumulation of active p-FAK Y397 at focal adhesions of cells cultured on Ti64, where it colocalized with the ends of actin stress fibers (figure 6). Peripheral localization of p-FAK Y397 was almost absent from cells cultured on Ti64 LP. Instead, the active form of the kinase showed diffuse cytoplasmic distribution, and only some minor localization with actin fibers was observed in attachment sites. p-FAK Y397 levels,

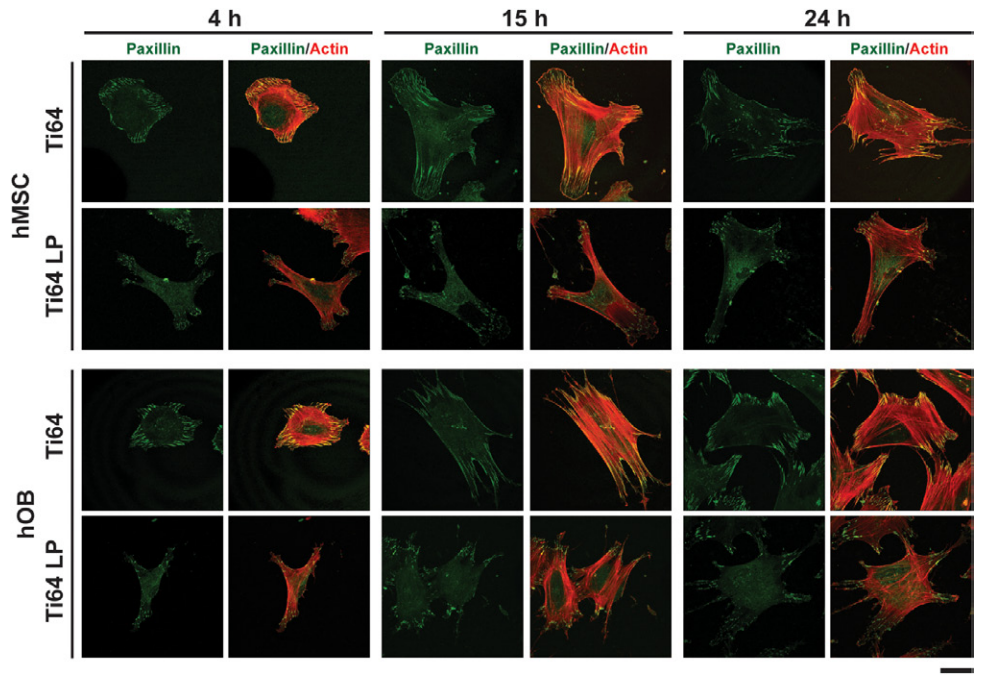

Figure 4. Pattern distribution of actin and paxillin in cells cultured on Ti64 LP surfaces. Confocal images showing paxillin (green) and the overlay (yellow) of paxillin (green) and actin (red) staining of hMSCs and hOBs cultured for 4, 15 and 24 h on Ti64 and Ti64 LP surfaces; bar, 40 μm. All images are representative of three independent experiments with similar results.

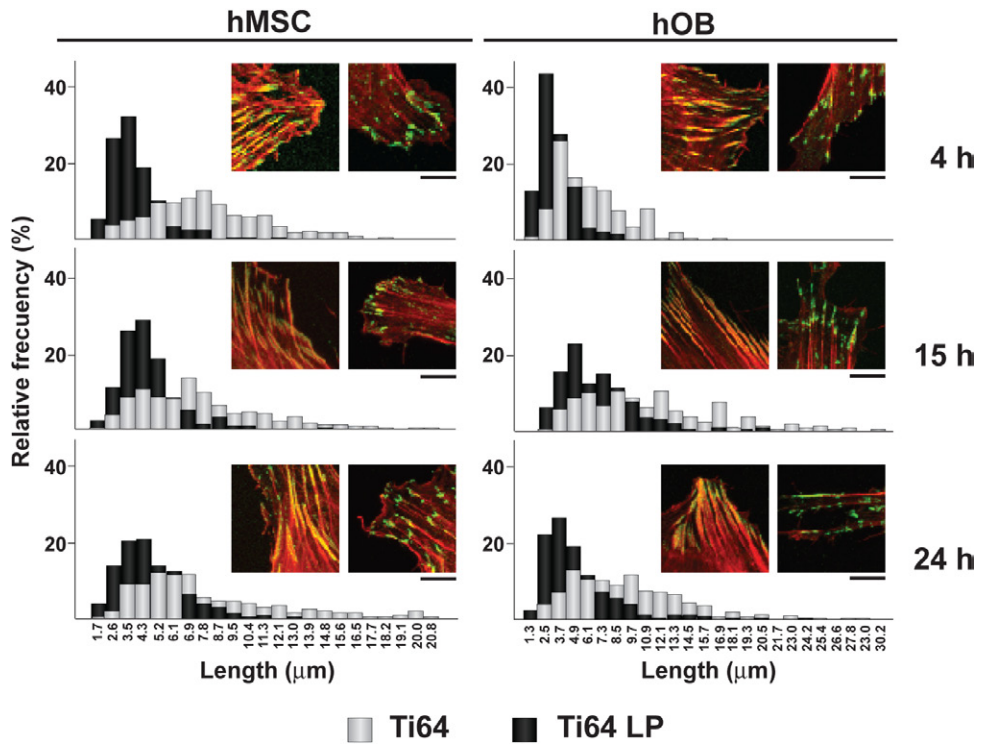

Figure 5. Length of paxillin in focal adhesions of cells cultured on Ti64 LP surfaces. Relative frequency histograms showing the length of paxillin in focal adhesions of hMSCs and hOBs cultured for 4, 15 and 24 h on Ti64 and Ti64 LP surfaces. The insets show the overlay (yellow) of actin (red) and paxillin (green) distribution in focal adhesions of cells cultured on Ti64 (left insets) or Ti64 LP (right insets); bar, 10 μm. All images are representative of three independent experiments with similar results.

quantified in protein extracts, were substantially lower in hMSCs and hOBs incubated on Ti64 LP than on Ti64 (figure 6). Next, we investigated whether the distribution pattern of p-FAK Y407 was modified in cells cultured on the treated alloy (figure 7). In hMSCs and hOBs incubated for 15 h on Ti64 and Ti64 LP, p-FAK Y407 exhibited a strong nuclear localization and more diffuse cytoplasmic distribution, with some small clusters associated with the end of stress fibers. A similar degree of colocalization of p-FAK Y407 and actin was

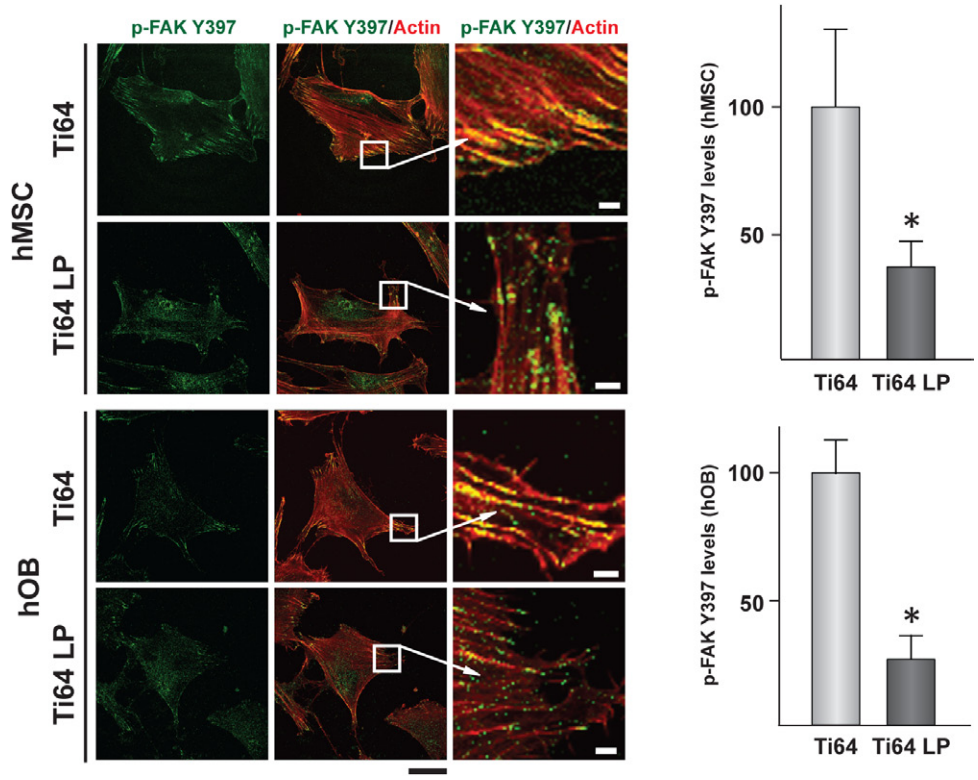

Figure 6. Localization pattern and levels of p-FAK Y397 in cells cultured on Ti64 LP surfaces. Left panel: confocal images showing p-FAK Y397 (green) and the overlay (yellow) of p-FAK Y397 (green) and actin (red) staining of hMSCs and hOBs cultured for 15 h on Ti64 and Ti64 LP surfaces; bar, 40 μm. Boxed areas are magnified on the right; bar, 4 μm. All images are representative of three independent experiments with similar results. Right panel: levels of p-FAK Y397 in hMSCs and hOBs cultured for 15 h on Ti64 and Ti64 LP surfaces. Data were normalized relative to the amounts of protein measured in cell layers from hMSCs and hOBs cultured on Ti64 surfaces, which were given an arbitrary value of 100 and corresponded to 0.24 $\pm$ 0.09 and 0.018 $\pm$ 0.002 U/μg total protein, respectively. Each bar graph represents the mean $\pm$ SD of six independent experiments. *$p < 0.05$ compared to cells cultured on Ti64 surfaces.

detected in the attachment sites of cells cultured on the treated or untreated alloy.

3.4. Cell viability and FN matrix organization on laser-peened Ti64 surfaces

hMSC and hOB viability increased over time regardless of the tested substrate (figure 8(a)). After 1 d of incubation, the metabolic activity of both cell types was slightly lower on Ti64 LP than on Ti64, while the numbers of cells adhered to the surfaces were similar. When incubation was prolonged to 4 and 7 d, no differences were observed between cells cultured on the untreated or treated alloy. A dense network of interconnected fibrils of FN was visible on the actin-stained monolayer of confluent hMSCs and hOBs cultured on the alloys for 7 d (figure 8(b)). No differences were observed in the organization of the meshwork of FN in cells incubated on Ti64 or Ti64 LP.

3.5. Cell differentiation and maturation on laser-peened Ti64 surfaces

Finally, cell layer differentiation and maturation were assessed in cultures of hMSCs and hOBs, respectively, which were incubated on the tested surfaces in osteogenic induction media (figure 9). An increase in ALP activity and extracellular matrix calcification were observed in hMSCs and hOBs as early as 13 d after incubation on Ti64 LP samples, as compared to Ti64. The morphology of the cell layers as well as osteocalcin deposition was investigated after 21 d of culturing. Visualization of actin filaments revealed that both cell types had condensed in clusters on the two studied surfaces. Osteocalcin staining within cell clusters was noticeably higher in hMSCs and hOBs cultured on Ti64 LP than on Ti64 samples (figure 9).

4. Discussion

To move forward the application of LP to the orthopaedic field, elimination of the sacrificial coating during processing of Ti64 is necessary to avoid toxicity effects associated with contamination of the alloy surface with impurities. When a nanosecond-order laser pulse focuses on a water-immersed metallic material, its outer layer absorbs the laser energy, causing important topographical and chemical changes of the surface. The results herein indicate that, as a consequence of temperature rise during laser focusing, melting and ablation generates an undulated surface. Also, LP notably modifies the surface chemistry of the alloy. There is an important increase of oxide layer thickness, which contains progressively less oxygen

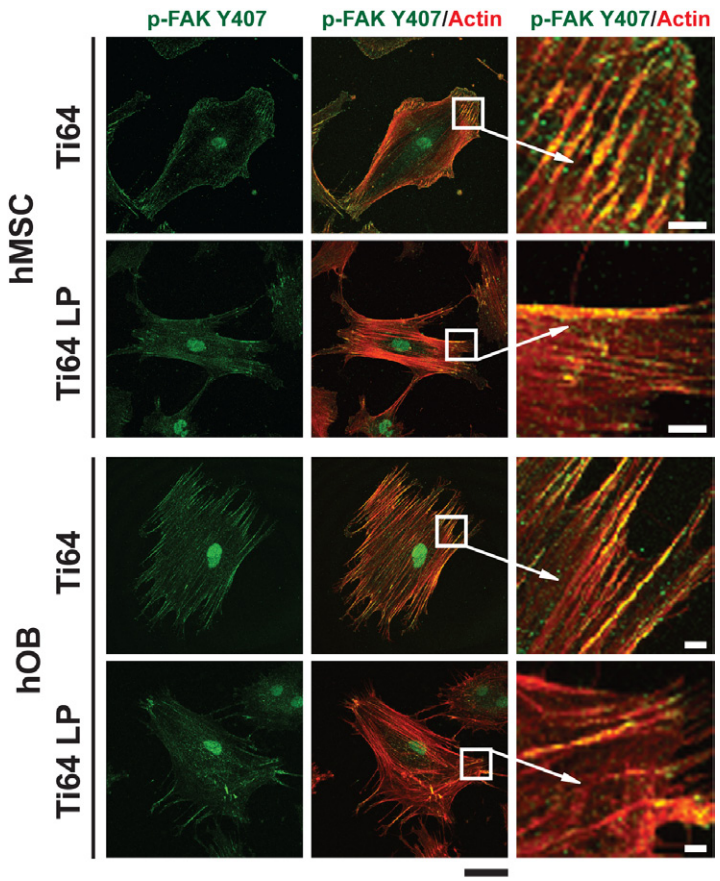

Figure 7. Localization pattern of p-FAK Y407 in cells cultured on Ti64 LP surfaces. Confocal images showing p-FAK Y407 (green) and the overlay (yellow) of p-FAK Y407 (green) and actin (red) staining of hMSCs and hOBs cultured for 15 h on Ti64 and Ti64 LP surfaces; bar, 40 μm. Boxed areas are magnified on the right; bar, 4 μm. All images are representative of three independent experiments with similar results.

on approaching the oxide layer–metal interface. In addition, the nature of the oxides in the Ti64 LP surface is different to that described in heated or anodized alloys. Also, water confinement allowed the most external enrichment in OH^- ions, some of them probably related to aluminium hydroxide.

The changes in composition and texture of the alloy surface may affect the adsorption and conformation of the adhesive proteins that establish the cell–alloy interface and, consequently, influence cell anchorage [22, 23]. Thermal oxidation of Ti64 in a furnace operating at 500–700 °C in air results in the formation of an outer layer of rutile that increases the adhesion rates of bone-forming cells to the alloy [2, 4, 8]. Unlike thermal treatment in air, which only marginally modifies surface roughness, LP treatment generates a wavy surface at a scale that can be recognized by hOBs and hMSCs [24]. Due to the significant physicochemical changes experienced by the LP-treated alloy surface, we surmised that cell adhesion rates would be significantly affected. Surprisingly, hOB and hMSC adhesion proceeded at the same rate in thermally oxidized Ti64 LP and Ti64. Despite the fact that there were no significant differences between the numbers of cells that adhered to the two alloys, hOBs and hMSCs reacted to the Ti64 LP surface with important morphological changes. After culturing for 4 h on flat Ti64 surfaces, cells were rounded, corresponding to cells that spread using mechanisms mainly mediated by lamellipodia [25]. These structures gradually disappeared as cell shape evolved to the typical morphologies characteristic of cells firmly adhered to the extracellular matrix. By contrast, cells cultured for 4 h on Ti64 LP were stretched and exhibited long filopodia, sensing structures that cells use to probe the extracellular matrix, identify suitable sites of adhesion and generate guidance cues for cell migration [26]. On the treated alloy, hOBs and hMSCs also developed noticeable lamellipodia, structures that enable crawling cells to steer, which were visible even after one day of culturing. Integrin-mediated interaction of cells with the extracellular matrix involves the formation of focal adhesions along the plasma membrane [27]. Comprised of clusters of integrin receptors associated with signalling, adaptor and structural proteins linked to the actin cytoskeleton, focal adhesions are highly and complex dynamic structures that involve a large number of molecules [28]. Among them, paxillin, a multidomain adaptor protein that recruits both structural and signalling molecules to focal adhesions [29], and FAK phosphorylated on residue 397, which directly interacts with downstream signalling molecules [30], are among the best understood. We have detected important changes in the focal adhesions of hOBs and hMSCs cultured on the treated alloy, which

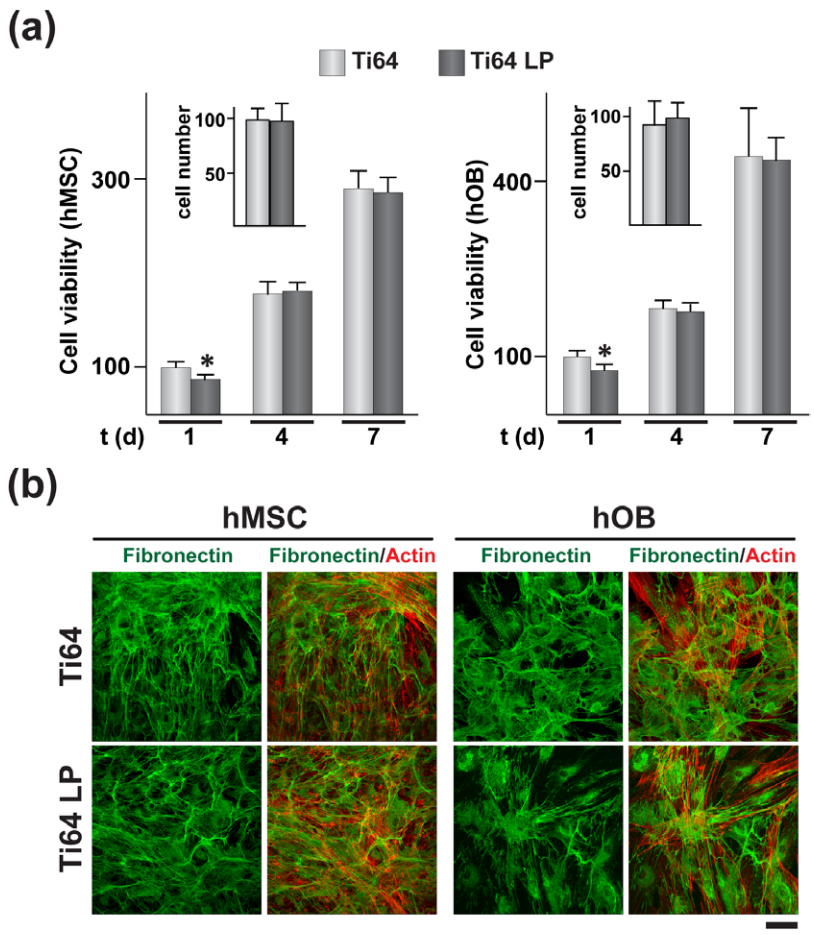

Figure 8. Cell viability and FN organization in cells cultured on Ti64 LP surfaces. (a) Cells were cultured for 1, 4 and 7 d on Ti64 and Ti64 LP surfaces. Viability data were normalized relative to the measured on Ti64 surfaces at day 1, which was given an arbitrary value of 100. The insets show the number of attached cells to a surface area of 727 $\times$ 727 μm^2 after 1 d of culture. Each value represents the mean $\pm$ SD of six independent experiments. *$p < 0.05$ compared to cells cultured on Ti64 surfaces. (b) Confocal images showing FN (green) and actin (red) staining of hMSCs and hOBs cultured for 7 d on Ti64 and Ti64 LP surfaces; bar, 40 μm. All images are representative of three independent experiments with similar results.

were smaller than in cells attached to the untreated alloy and showed a marked loss of colocalization of actin fibers with paxillin and p-FAK Y397. In addition, p-FAK Y397 levels substantially diminished in hOBs and hMSCs grown on Ti64 LP. Phosphorylation of FAK on residue 407 negatively regulates the adhesion-mediated activity of the kinase and decreases its autophosphorylation on residue 397 [31]. Strikingly, p-FAK Y407 similarly colocalized with actin in cells cultured on Ti64 or Ti64 LP, indicating an important imbalance of phosphorylation and/or dephosphorylation of FAK in cells attached to the treated alloy.

All these changes in cell adhesion to Ti64 LP are intriguing and their biological significance remains to be elucidated. Cells lacking important components of focal adhesions can adhere to metallic substrates. Thus, FAK null fibroblasts attach to polished and sandblasted titanium, likely through an enrichment of cortactin at the adhesion sites [32]. As an inverse correlation between the size and organization of focal adhesions and cell migration speed has been generally reported [33], the observed alterations suggest that cell migration may be more active on LP-treated alloy than on the untreated surface. The nature of the titanium oxide layers developed on the surface of Ti64 by means of e.g. anodic oxidation or thermal oxidation has been claimed to influence the adhesive and migratory cell behaviour. Thus, osteoblastic human Saos-2 cells attached to anodically oxidized Ti64 also display defective staining of vinculin, an actin-binding protein enriched in focal adhesion sites, and develop more lamellipodia than in the untreated alloy [34]. However, p-FAK Y397 was detected as large patches at the adhesion sites of hOBs attached to Ti64 thermally oxidized in air [8]. Oxidation of the surface of Ti-based materials involves, to a greater or lesser extent, changes in its topography [8, 34]. Consequently, cell adhesion behavior on oxidized Ti64 cannot be exclusively ascribed to alterations in surface chemistry. The spatial organization of focal adhesions on metallic materials with deformed surfaces has been also the subject of previous studies. Similarly to what we have observed, murine osteoblastic MC3T3-E1 cells cultured on sandblasted and acid-etched Ti surfaces develop long cytoplasmic protrusions [35]. Also, osteoblastic human MG-63 cells exhibit reduced numbers of adhesions with smaller size on corundum

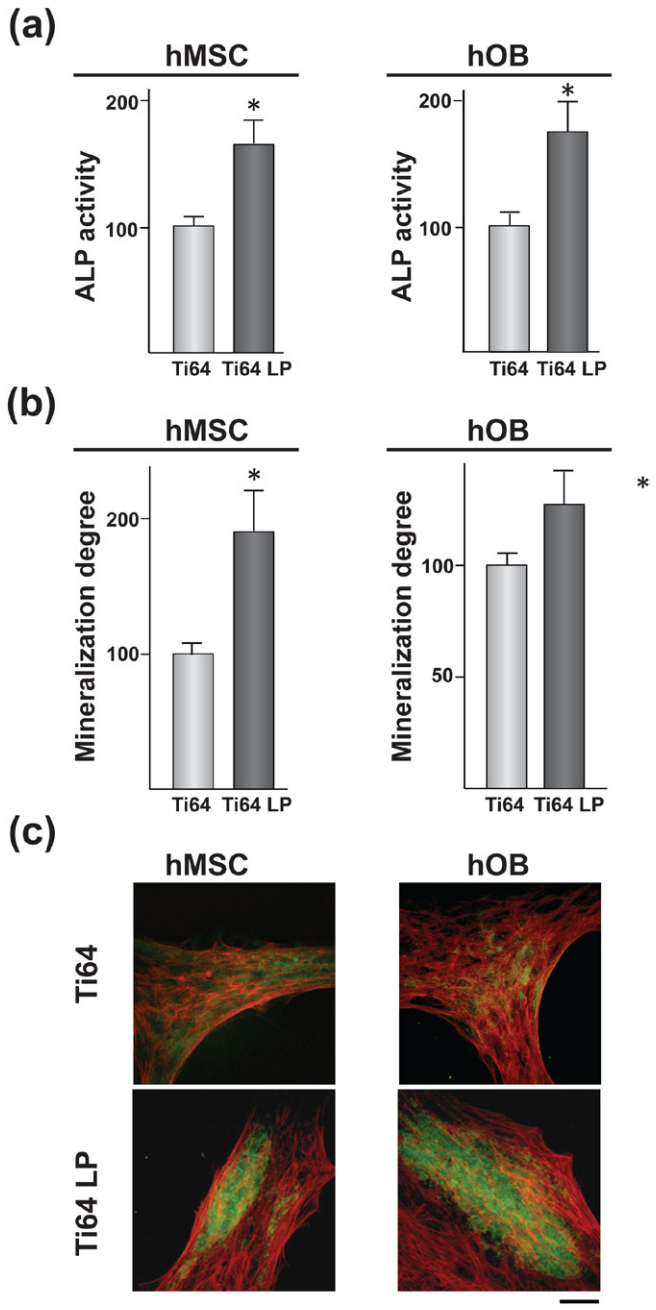

Figure 9. hMSC differentiation and hOB maturation on Ti64 LP surfaces. (a) ALP activity and (b) cell layer calcification of hMSCs and hOBs cultured for 13 d in osteogenic media on Ti64 and Ti64 PL surfaces. ALP activity and cell layer mineralization data were normalized relative to the activities and absorbances, respectively, measured in cells cultured on Ti64 surfaces, which were given an arbitrary value of 100. A relative value of ALP activity of 100 corresponded to 17.4 ± 1.2 and 97.9 ± 4.9 nmol *p*-nitrophenol/mg protein min^{-1} in hMSCs and hOBs, respectively. Each value represents the mean ± SD of six independent experiments. *$p < 0.05$ compared to cells cultured on Ti64 surfaces. (c) Confocal images showing osteocalcin (green) and actin (red) staining of hMSCs and hOBs cultured for 21 d on Ti64 and Ti64 PL surfaces in osteogenic media; bar, 100 μm. All images are representative of three independent experiments with similar results.

blasted than on polished Ti surfaces [36, 37], and similar observations were made in human fetal-osteoblast hFOB 1.19 cells cultured on anodized rough Ti substrates [38]. Methods employed in the metallurgy field to increase the surface roughness of Ti64 alloy, such as surface machining, acid etching, sandblasting or plasma-spraying, unavoidably result in significant changes of surface composition, which makes it difficult to elucidate the relative topological contribution of the surface to cell adhesive behavior [39, 40]. Therefore, it cannot be unambiguously clarified whether changes in surface chemistry or roughness, or a combined effect of the two, underlie the cell responses to the oxidized and rough Ti64 LP surface.

Although mechanisms of adhesion are deeply affected, the metabolic activities of hOBs and hMSCs cultured on the LP-treated or untreated alloy increased as a function of time with a similar rate. That the treated alloy promotes cell colonization and proliferation was confirmed by immunostaining using a human FN antibody, which revealed that cells can reach confluence and organize a dense network of extracellular

matrix. Polished Ti64 allows the osteogenic differentiation of hMSCs as well as the maturation of hOBs [2, 8, 20, 40, 41]. Differentiation of osteoprogenitor cells towards the osteoblastic phenotype was higher in the treated than on the untreated surface, as indicated by the measurements of ALP activity and matrix calcification of hMSCs cultured in media containing osteogenic inducers. Osteocalcin, a protein primarily secreted by osteoblasts that binds to hydroxyapatite during bone matrix mineralization [42], was deposited by hMSCs to a greater extent on Ti64 LP than on Ti64. Also, the specific functions of human osteoblasts were enhanced when cultured in osteogenic media on Ti64 LP. In addition to the influence that the chemistry of the treated alloy surface may exert on the cell response to the inducers of osteoblast differentiation, its undulated surface may also play a critical role. Much better bone fixation is achieved with rough than smooth Ti-based alloys [43], an effect related to increased specific activities of bone-forming cells on materials displaying micrometer or submicrometer scale surface roughness [2, 8, 44, 45]. The mechanisms that led to enhanced differentiation in cells cultured on Ti64 LP, a surface that leads to important alterations in cell adhesion, remain to be analyzed. It is known that initial cell adhesion on Ti-based materials does not necessarily correlate with the cell behaviour in the long term [46]; i.e. unfavourable or delayed cell attachment can precede enhanced cell proliferation and/or differentiation. There are previous studies reporting impaired adhesion, e.g. altered cell spreading or cytoskeletal reorganization, on rough Ti-based materials, which is followed by increased expression of osteoblastic differentiation markers [2, 45, 47]. Impaired organization of focal adhesions in cells attached to Ti-based surfaces, similar to what we have observed in Ti64 LP, has been described in previous studies which reported no changes in ALP activity [34, 38] or an increase in the expression of the osteoblastic differentiation marker bone sialoprotein [37]. Unfortunately, these studies were conducted with osteoblastic cell lines cultured in the absence of osteogenic inducers, making any correlation with the data presented here, obtained with primary cells cultured with dexamethasone, β-glycerol phosphate and ascorbic acid, difficult. Cell adhesion and osteoblast differentiation can occur in the total absence of FAK activation. Thus, FAK null osteoblasts can attach to standard tissue culture plastic (TCP), exhibiting actin fiber and focal adhesion formation, although the number of focal adhesions in these cells is lower than in wild-type cells [48]. Apart from FAK, multiple signalling proteins can be recruited to focal adhesions, including serine–threonine and tyrosine kinases, protein phosphatases, Rho GTPases and adapter proteins containing protein–protein binding domains [49]. That the loss of FAK may not be critical for *in vitro* osteoblast differentiation was demonstrated in murine FAK null cells derived from calvaria and from bone marrow, which differentiated to osteoblasts when cultured on TCP in osteogenic media [50]. In these cells, the active form of the tyrosine kinase Pyk2 localizes in the focal adhesions, where it may replace some of the functions of the deleted FAK in the process of osteoblast differentiation [50]. Another downstream pathway of focal adhesions is mediated by the integrin-linked kinase (ILK), which promotes osteoblast differentiation on rough Ti-based substrates, where attached cells exhibit numerous filopodia and lamellipodia protrusions [51, 52]. FAK activation is reduced but not completely lost in hMSCs and hOBs cultured on Ti64 LP. We hypothesize that Pyk2, ILK or other signalling proteins may balance the diminished FAK activation of cells attached to Ti64 LP, allowing the process of osteoblast differentiation that is enhanced by the physicochemical characteristics of the alloy surface.

In summary, this study indicates that LP is an efficient method to oxidize the Ti64 surface in the absence of sacrificial layers. The treatment tailors the alloy surface to yield a thick oxidized layer with increased roughness that supports the colonization and activities of bone-lineage cells. Interestingly, LP is suitable for treating local areas of a component and may target confined regions inaccessible to other technologies. Additional advantages in terms of the expected increase in the fatigue strength and suppression of ion release cannot be ignored. The treatment could also be advantageously applied to blasted Ti64 to generate an outer oxidized layer and improve its mechanical properties, as remnant particles embedded after blasting act as stress concentrators that decrease the fatigue life of the alloy.

5. Conclusion

Treatment of Ti64 by means of LP in the absence of sacrificial coatings generates a rough surface that exhibits an important increase in the content of titanium oxides and OH− ions. Adhesion of human mesenchymal stem cells and osteoblasts to the treated alloy is deeply affected, including morphological changes as well as important alterations in the formation of focal adhesions. However, cells attach and proliferate on the treated alloy at the same rate as on the untreated surface. Human mesenchymal cells cultured in media containing osteogenic inducers on the treated alloy differentiate towards the osteoblastic phenotype to a higher extent than on the untreated surface, and the specific functions of human osteoblasts cultured on these media are also enhanced on the treated alloy. These findings indicate that thermal oxidation of Ti64 by means of LP is a suitable technology to generate surfaces that promote the responses of bone-lineage cells.

Acknowledgments

The authors are greatly indebted to J Rams and A J Lopez-Galisteo (Universidad Rey Juan Carlos, Madrid) for excellent help with optical profilometry. We also acknowledge technical assistance by F Bensiamar

(Hospital Universitario La Paz-IdiPAZ and CIBER-BBN). XPS and TofSIMS analyses were performed by the SCC Unit at the ICTS 'NANOBIOSIS'of CIBER-BBN at the SAIUEX (University of Extremadura). This work was supported by grants PI12/01698 from Fondo de Investigaciones Sanitarias (FIS, Spanish Ministry of Economy and Competitiveness, MINECO, Spain), S2013/MIT-2862 from Comunidad de Madrid, MAT2009-14695-C04-01-02-04 from the former Spanish Ministry of Science and Innovation (MICINN), MAT2012-37736-C05-03-05 and MAT2014-52905-REDT (MINECO) and GR10149 (Junta de Extremadura, Spain). LC was the recipient of predoctoral fellowship BES-2010-034989 from MICINN. LS is supported by grant award CP11/00022 (FIS). NV is supported by Program I2 from Comunidad de Madrid (Spain).

References

[1] Browne M and Gregson P J 1994 Surface modification of titanium alloy implants *Biomaterials* **15** 894–8
[2] Saldaña L, Barranco V, González-Carrasco J L, Rodríguez M, Munuera L and Vilaboa N 2007 Thermal oxidation enhances early interactions between human osteoblasts and alumina blasted Ti6Al4V alloy *J. Biomed. Mater. Res.* A **81A** 334–46
[3] Saldaña L, Barranco V, García-Alonso M C, Vallés G, Escudero M L, Munuera L and Vilaboa N 2006 Concentration-dependent effects of titanium and aluminium ions released from thermally oxidized Ti6Al4V alloy on human osteoblasts *J. Biomed. Mater. Res.* A **77** 220–9
[4] García-Alonso M C, Saldaña L, Vallés G, González-Carrasco J L, González-Cabrero J, Martínez M E, Gil-Garay E and Munuera L 2003 *In vitro* corrosion behaviour and osteoblast responses of thermally oxidised Ti6Al4V alloy *Biomaterials* **24** 19–26
[5] Barranco V, Escudero M L and García-Alonso M C 2007 3D, chemical and electrochemical characterization of blasted Ti6Al4V surfaces: its influence on the corrosion behaviour *Electrochim. Acta* **52** 4374–84
[6] Barranco V, Onofre E, Escudero M L and García-Alonso M C 2010 Characterization of roughness and pitting corrosion of surfaces modified by blasting and thermal oxidation *Surf. Coat. Technol.* **204** 3783–93
[7] Barranco V, Escudero M L and García-Alonso M C 2011 Influence of the microstructure and topography on the barrier properties of oxide scales generated on blasted Ti6Al4V surfaces *Acta Biomater.* **7** 2716–25
[8] Saldaña L, Vilaboa N, Vallés G, González-Cabrero J and Munuera L 2005 Osteoblast response to thermally oxidized Ti6Al4V alloy *J. Biomed. Mater. Res.* A **73** 97–107
[9] Montross C S, Wei T, Ye L, Clark G and Mai Y-W 2002 Laser shock processing and its effects on microstructure and properties of metal alloys: a review *Int. J. Fatigue* **24** 1021–36
[10] Multigner M, Frutos E, Mera C L, Chao J and Gonzalez-Carrasco J L 2009 Interrogations on the sub-surface strain hardening of grit blasted Ti-6Al-4V alloy *Surf. Coat. Technol.* **203** 2036–40
[11] Ashley S 1998 Powerful laser means better peening *Mech. Eng.* **120** 12
[12] Peyre P, Fabbro R, Merrien P, Lieurade H P 1996 Laser shock processing of aluminium alloys. Application to high cycle fatigue behaviour *Mater. Sci. Eng.* A **210** 102–13
[13] Magnissalis E A, Zinelis S, Karachalios T and Hartofilakidis G 2003 Failure analysis of two Ti-alloy total hip arthroplasty femoral stems fractured *in vivo J. Biomed. Mater. Res.* B **66** 299–305
[14] Chao J and López V 2007 Failure analysis of a Ti6Al4V cementless HIP prosthesis *Eng. Fail. Anal.* **14** 822–30
[15] Baxmann M, Jauch S Y, Schilling C, Blömer W, Grupp T M and Morlock M M 2013 The influence of contact conditions and micromotions on the fretting behavior of modular titanium alloy taper connections *Med. Eng. Phys.* **35** 676–83
[16] Shemtov-Yona K and Rittel D 2014 Identification of failure mechanisms in retrieved fractured dental implants *Eng. Fail. Anal.* **38** 58–65
[17] Nalla R K, Altenberger I, Noster U, Liu G Y, Scholtes B and Ritchie R O 2003 On the influence of mechanical surface treatments—deep rolling and laser shock peening—on the fatigue behavior of Ti/6Al/4V at ambient and elevated temperatures *Mater. Sci. Eng.* A **355** 216–30
[18] Guo Y B and Caslaru R 2011 Fabrication and characterization of micro dent arrays produced by laser shock peening on titanium Ti-6Al-4V surfaces *J. Mater. Process. Technol.* **211** 729–36
[19] Altenberger I, Nalla R K, Sano Y, Wagner L and Ritchie R O 2012 On the effect of deep-rolling and laser-peening on the stress-controlled low- and high-cycle fatigue behavior of Ti-6Al-4V at elevated temperatures up to 550 degrees C *Int. J. Fatigue* **44** 292–302
[20] Calzado-Martín A, Crespo L, Saldaña L, Boré A, Gómez-Barrena E and Vilaboa N 2014 Human bone-lineage cell responses to anisotropic Ti6Al4V surfaces are dependent on their maturation state *J. Biomed. Mater. Res.* A **102** 3154–66
[21] Hung P S, Kuo Y C, Chen H G, Chiang H H and Lee O K 2013 Detection of osteogenic differentiation by differential mineralized matrix production in mesenchymal stromal cells by Raman spectroscopy *PLoS One* **8** e65438
[22] Deligianni D D, Katsala N, Ladas S, Sotiropoulou D, Amedee J and Missirlis Y F 2001 Effect of surface roughness of the titanium alloy Ti-6Al-4V on human bone marrow cell response and on protein adsorption *Biomaterials* **22** 1241–51
[23] MacDonald D E, Rapuano B E, Deo N, Stranick M, Somasundaran P and Boskey A L 2004 Thermal and chemical modification of titanium–aluminum–vanadium implant materials: effects on surface properties, glycoprotein adsorption, and MG63 cell attachment *Biomaterials* **25** 3135–46
[24] Anselme K 2011 Biomaterials and interface with bone *Osteoporos. Int.* **22** 2037–42
[25] Small J V, Stradal T, Vignal E and Rottner K 2002 The lamellipodium: where motility begins *Trends Cell Biol.* **12** 112–20
[26] Partridge M A and Marcantonio E E 2006 Initiation of attachment and generation of mature focal adhesions by integrin-containing filopodia in cell spreading *Mol. Biol. Cell.* **17** 4237–48
[27] Sastry S K and Burridge K 2000 Focal adhesions: a nexus for intracellular signaling and cytoskeletal dynamics *Exp. Cell Res.* **261** 25–36
[28] Huttenlocher A and Horwitz A R 2011 Integrins in cell migration *Cold Spring Harb. Perspect. Biol.* **3** a005074
[29] Brown M C and Turner C E 2004 Paxillin: adapting to change *Physiol. Rev.* **84** 1315–39
[30] Mitra S K, Hanson D A and Schlaepfer D D 2005 Focal adhesion kinase: in command and control of cell motility *Nat. Rev. Mol. Cell Biol.* **6** 56–68
[31] Lim Y, Park H, Jeon J, Han I, Kim J, Jho E H and Oh E S 2007 Focal adhesion kinase is negatively regulated by phosphorylation at tyrosine 407 *J. Biol. Chem.* **282** 10398–404
[32] Oates C J, Wen W and Hamilton W 2011 Role of titanium surface topography and surface wettability on focal adhesion kinase mediated signaling in fibroblasts *Materials* **4** 893–907
[33] Lauffenburger D A and Horwitz A F 1996 Cell migration: a physically integrated molecular process *Cell* **84** 359–69
[34] Zhu X, Chen J, Scheideler L, Reichl R and Geis-Gerstorfer J 2004 Effects of topography and composition of titanium surface oxides on osteoblast responses *Biomaterials* **25** 4087–103
[35] Le Guehennec L, Lopez-Heredia M A, Enkel B, Weiss P, Amouriq Y and Layrolle P 2008 Osteoblastic cell behaviour on different titanium implant surfaces *Acta Biomater.* **4** 535–43

[36] Diener A, Nebe B, Lüthen F, Becker P, Beck U, Neumann H G and Rychly J 2005 Control of focal adhesion dynamics by material surface characteristics *Biomaterials* **26** 383–92
[37] Nebe J G, Luethen F, Lange R and Beck U 2007 Interface interactions of osteoblasts with structured titanium and the correlation between physicochemical characteristics and cell biological parameters *Macromol. Biosci.* **7** 567–78
[38] Setzer B, Bächle M, Metzger M C and Kohal R J 2009 The gene-expression and phenotypic response of hFOB 1.19 osteoblasts to surface-modified titanium and zirconia *Biomaterials* **30** 979–90
[39] Anselme K, Linez P, Bigerelle M, Le Maguer D, Le Maguer A, Hardouin P, Hildebrand H F, Iost A and Leroy J M 2000 The relative influence of the topography and chemistry of TiAl6V4 surfaces on osteoblastic cell behaviour *Biomaterials* **21** 1567–77
[40] Anselme K and Bigerelle M 2014 On the relation between surface roughness of metallic substrates and adhesion of human primary bone cells *Scanning* **36** 11–20
[41] Saldaña L, Méndez-Vilas A, Jiang L, Multigner M, González-Carrasco J L, Pérez-Prado M T, González-Martín M L, Munuera L and Vilaboa N 2007 *In vitro* biocompatibility of an ultrafine grained zirconium *Biomaterials* **28** 4343–54
[42] Lian J B and Stein G S 1992 Concepts of osteoblast growth and differentiation: basis for modulation of bone cell development and tissue formation *Crit. Rev. Oral Biol. Med.* **3** 269–305
[43] Le Guéhennec L, Soueidan A, Layrolle P and Amouriq Y 2007 Surface treatments of titanium dental implants for rapid osseointegration *Dent. Mater.* **23** 844–54
[44] Gittens R A, McLachlan T, Olivares-Navarrete R, Cai Y, Berner S, Tannenbaum R, Schwartz Z, Sandhage K H and Boyan B D 2011 The effects of combined micron-/submicron-scale surface roughness and nanoscale features on cell proliferation and differentiation *Biomaterials* **32** 3395–403
[45] Olivares-Navarrete R, Hyzy S L, Berg M E, Schneider J M, Hotchkiss K, Schwartz Z and Boyan B D 2014 Osteoblast lineage cells can discriminate microscale topographic features on titanium-aluminum-vanadium surfaces *Ann. Biomed. Eng.* **42** 2551–61
[46] Bigerelle M and Anselme K 2005 Bootstrap analysis of the relation between initial adhesive events and long-term cellular functions of human osteoblasts cultured on biocompatible metallic substrates *Acta Biomater.* **1** 499–510
[47] Saldaña L, Gonzalez-Carrasco J L, Rodríguez M, Munuera L and Vilaboa N 2006 Osteoblast response to plasma-spray porous Ti6Al4V coating on substrates of identical alloy *J. Biomed. Mater. Res.* A **77** 608–17
[48] Castillo A B *et al* 2012 Focal adhesion kinase plays a role in osteoblast mechanotransduction *in vitro* but does not affect load-induced bone formation *in vivo PLoS One* **7** e43291
[49] Rottner K and Stradal T E 2011 Actin dynamics and turnover in cell motility *Curr. Opin. Cell Biol.* **23** 569–78
[50] Kim J B, Leucht P, Luppen C A, Park Y J, Beggs H E, Damsky C H and Helms J A 2007 Reconciling the roles of FAK in osteoblast differentiation, osteoclast remodeling, and bone regeneration *Bone* **41** 39–51
[51] Wang W, Zhao L, Wu K, Ma Q, Mei S, Chu P K, Wang Q and Zhang Y 2013 The role of integrin-linked kinase/β-catenin pathway in the enhanced MG63 differentiation by micro/nano-textured topography *Biomaterials* **34** 631–40
[52] Wang W, Liu Q, Zhang Y and Zhao L 2014 Involvement of ILK/ERK1/2 and ILK/p38 pathways in mediating the enhanced osteoblast differentiation by micro/nanotopography *Acta Biomater.* **10** 3705–15